ACS OMEGA

http://pubs.acs.org/journal/acsodf

Article

Antibacterial Nanoparticles with Natural Photosensitizers Extracted from Spinach Leaves

Pavel Ludačka, Pavel Kubát,* Zuzana Bosáková, and Jiří Mosinger*

Cite This: *ACS Omega* 2022, 7, 1505−1513

Read Online

ACCESS | Metrics & More | Article Recommendations | Supporting Information

ABSTRACT: We prepared antibacterial polystyrene nanoparticles (NPs) with natural photosensitizers from chlorophyll (Chl) extract via a simple nanoprecipitation method using the same solvent for dissolution of the polystyrene matrix and extraction of Chls from spinach leaves. A high photo-oxidation and antibacterial effect was demonstrated on *Escherichia coli* and was based on the photo-generation of singlet oxygen $O_2(^1\Delta_g)$, which was directly monitored by NIR luminescence measurements and indirectly verified using a chemical trap. The photoactivity of NPs was triggered by visible light, with enhanced red absorption by Chls. To reduce the quenching effect of carotenoids (β-carotene, lutein, etc.) in the Chl extract, diluted and/or preirradiated samples, in which the photo-oxidized carotenoids lose their quenching effect, were used for preparation of the NPs. For enhanced photo-oxidation and antibacterial effects, a sulfonated polystyrene matrix was used for preparation of a stable dispersion of sulfonated NPs, with the quenching effect of carotenoids being suppressed.

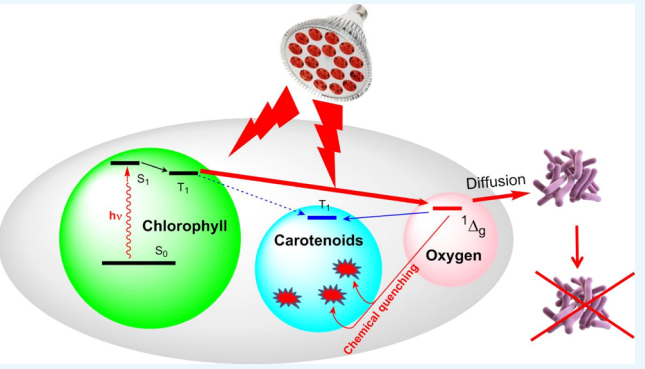

INTRODUCTION

Chlorophylls (Chls) are widely abundant photosensitizers in nature that enable conversion of solar energy to biochemically useful forms.[1,2] They are very cheap, commercially available, main group metal-based, and provide excellent efficiency for singlet oxygen-mediated chemistry.[3] The photosensitization process from the S_1 states after excitation with red and/or blue radiation competes with a very efficient intersystem crossing to the T_1 state and the formation of highly reactive singlet oxygen $[O_2(^1\Delta_g)]$. In general, $O_2(^1\Delta_g)$ is generated during photosynthesis in the photosystem II center.[4,5] It is a signal molecule, but at high concentrations, it can oxidize and destroy target structures and can be applied for photodynamic inactivation of bacteria and viruses[6,7] and for photodynamic therapy to treat tumors.[8,9]

Chl extract from spinach (ChlE) and other plants is highly promising for applications in reactions photosensitized by $O_2(^1\Delta_g)$. A recent paper[10] reported quantum yield of singlet oxygen $\Phi_\Delta = 0.58$ for a Chl-based extract, similar to the value of $\Phi_\Delta = 0.51$ for Chl *a*. Note that Φ_Δ values for Chl-based compounds in different solvents were summarized in previous comprehensive reviews published more than 20 years ago.[11,12] Application of the extract is limited by the presence of carotenoids that dramatically decrease photo-oxidation efficiency,[13] which is a harmful process for natural or artificial photosynthesis.[14,15] Both Chl triplet states and $O_2(^1\Delta_g)$ can be quenched by carotenoids via energy transfer (physical quenching). Additionally, carotenoids (carotenes and xanthophylls)[16] quench $O_2(^1\Delta_g)$ in a chemical way to form endoperoxides as a major oxidation product by cleavage of double bonds of the polyene chain, resulting in a variety of aldehydes with different chain lengths.[17] Carotenoids also have a positive role; they absorb visible light in the blue-green region, in which Chls have a low extinction coefficient, and transfer excitation energy to Chls.[18] Another undesirable property of the Chl extract from green plants is its degradation upon irradiation with light. Thus, improving the Chl photostability is necessary to facilitate its biomedical application.[19] Heavy metal-substituted Chls can be more stable than natural magnesium Chls[20] but exhibit a lower $O_2(^1\Delta_g)$ production efficiency than Mg or Zn derivatives.[21]

Isolation of pure photosensitizers from ChlE requires complicated purification methods and toxic solvents to isolate individual photosensitizers. Chl s can also be used as starting materials for the synthesis of functionalized chlorins[22] to improve photodynamic activity. Previous studies[10,23] indicate that ChlE itself can be an excellent "green" photosensitizer for environmental applications, even in the presence of carote-

Received: November 8, 2021
Accepted: December 8, 2021
Published: December 17, 2021

https://doi.org/10.1021/acsomega.1c06229
ACS Omega 2022, 7, 1505−1513

noids that are diluted in solutions in comparison with their level in plants.

There are plenty of organic and inorganic nanocarriers under investigation for transport of photosensitizers, some of them have good photocatalytic and/or antibacterial properties.[24] In our previous studies, we prepared different nanofiber materials[25] and nanoparticles (NPs)[26] with a porphyrin photosensitizer, which generated $O_2(^1\Delta_g)$ "on demand" after excitation with visible light and exhibited antibacterial properties. In general, NPs with a high surface/volume ratio photogenerate a high amount of $O_2(^1\Delta_g)$ and can move in close proximity to the biological targets to be destroyed, which can overcome the $O_2(^1\Delta_g)$ diffusion limitations. The encapsulated photosensitizer is well protected against external quenchers, which allows quenching of triplet states by oxygen, exclusively in the interior of NPs. These antibacterial NPs are considered an alternative to antibiotics and have strong potential to solve the problem of bacterial multidrug resistance.[27]

Among the variety of nanocarriers suitable for photodynamic inactivation, polystyrene NPs are superior due to their biocompatibility, low toxicity, high oxygen permeability/diffusion coefficient, and negligible leakage of nonpolar encapsulated photosensitizes to aqueous media.[28]

This report describes a simple method for preparation of an aqueous dispersion of polystyrene NPs with encapsulated ChlE from spinach (*Spinacia oleracea*). In addition to Chl, the extract also contained carotenoids, which have a negative influence on photoactive NPs with respect to their photo-oxidation, antibacterial activity, and photostability. We used three simple methods to suppress the quenching effect of carotenoids: working with diluted ChlE (i), using ChlE preirradiated with light to photo-oxidize the carotenoids (ii), and/or using small sulfonated polystyrene NPs with a higher surface/volume ratio to suppress the effect of carotenoids inside the NPs (iii). The main advantages of this approach in the synthesis of photoactive NPs are the application of a "green" photosensitizer abundant in nature with absorption in both the red and blue regions of the visible spectrum and using the same solvent for extraction of Chl and preparation of NPs. Moreover, glassy polystyrene NPs prepared by the nanoprecipitation method are more stable than liposome- or polymeric micelle-based NPs[10,29,30] and should preserve favorable photophysical properties not influenced by photoelectron transfer from excited Chl molecules to the metal core typically for gold[31] and silver[32] NPs.

RESULTS AND DISCUSSION

ChlE High-Performance Liquid Chromatography Analysis. Chl *a* and Chl *b* are highly abundant in green leaves and are accompanied by protective carotenoids.[33] HPLC analysis revealed that the retention times and mass spectrometry (MS) profiles of compounds found in ChlE correspond to Chl *a*, Chl *b*, *β*-carotene, and lutein standards (Table 1, Figure S1, panel B, and Figure S2 in Supporting Information).

For HPLC quantitative estimation, a mixture of standards (Chl *a*, Chl *b*, *β*-carotene, and lutein) at concentrations of 0.5, 1, 2.5, 5, and 7.5 mg/L, respectively, in MeOH/THF 9:1 (v/v) was applied and used to construct calibration plots for each component (peak area *vs.* concentration). Then, ChlE diluted 10× in MeOH was tested. The concentration of each component was estimated from calibration plots (Table 1). Evidently, Chl *a* is the main compound in ChlE.

Table 1. Retention Time of Standards and Concentration of Corresponding Compounds in ChlE[a]

pigment	Chl *a*	Chl *b*	*β*-carotene	lutein
t_R (min)	17.6	9.8	56.7	4.3
c (mg/l)	154 (190)	54 (62)	38	28 (39)
content in w/w %	56 (58)	20 (19)	14 (11)	10 (12)

[a]The values in parentheses include the isomers of the respective compounds.

Note that the amount/concentration of Chl photosensitizers and carotenoids in ChlE depends on the species of green plant and changes during a season.[34]

Spectroscopic and Photophysical Properties. The UV−vis absorption spectrum of THF extract prepared from spinach (ChlE) was compared with that of Chl *a*, Chl *b*, *β*-carotene, and lutein standards (Figure 1A). The spectrum of

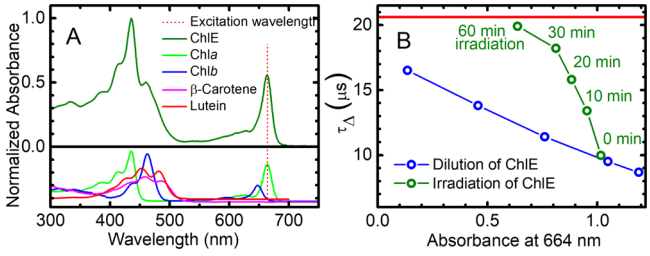

Figure 1. (A) Normalized UV/vis spectrum of ChlE in tetrahydrofuran (THF) compared with the Chl *a*, Chl *b*, *β*-carotene, and lutein spectra. (B) Dependence of singlet oxygen lifetime (τ_Δ) on the absorbance in the Q_y band after dilution of original ChlE, and after irradiation of ChlE with a 250 W Xe lamp with a long pass filter ($\lambda \geq$ 400 nm). The red line corresponds to τ_Δ in THF measured for standard ZnPc and Chl *a* photosensitizers.

ChlE consists of a Q_y band of Chls at 664 nm corresponding predominantly to the Chl *a* spectrum and of a Soret band in the blue region of the spectrum partially overlaid with the absorption band of other species (Chl *b*, carotenoids, etc.). The absorption spectrum allows efficient harvesting of red and blue radiation in the solar spectrum.

We measured the weak near infrared luminescence of singlet oxygen, $O_2(^1\Delta_g)$ at ∼1270 nm (Figure S3 and S4 in Supporting Information) and estimated the quantum yield (Φ_Δ) by comparing the amplitudes of singlet oxygen decay kinetics after excitation with a dye laser (664 nm and 28 ns pulse length) at the same absorbance at the excitation wavelength (Table 2).

Taking into account Φ_Δ = 0.53 for ZnPc in THF,[35] the calculated values of Φ_Δ were 0.64 and 0.66 for ChlE and Chl *a*, respectively. This result corresponds to previous literature data for ChlE prepared from spinach.[10]

The concentration of photosensitizers (predominantly Chl *a*) used in experiments was proportional to the absorbance at the Q_y band of Chl. The estimated concentration was 10^{-5} mol.L^{-1} (Table S1 in Supporting Information) or lower taking into account the literature value for the extinction coefficient of Chl *a* (∼9 × 10^5 L mol^{-1} cm^{-1}). The singlet oxygen lifetime (τ_Δ) increased with the dilution of ChlE due to the lower concentration of quenchers (carotenoids, Figure 1B).

https://doi.org/10.1021/acsomega.1c06229
ACS Omega 2022, 7, 1505−1513

Table 2. Photophysical Parameters: Lifetime of Singlet Oxygen in THF (τ_Δ), the Quantum Yield of Singlet Oxygen (Φ_Δ), Lifetime of the Chl Triplet States in Argon (τ_0)- and Air (τ_{air})-Saturated THF and the Fraction of the Triplet States Quenched by Oxygen in Air-Saturated Solution ($F_T = 1 - \tau_0/\tau_{Air}$)

	singlet oxygen	triplet states			
	τ_Δ (μs)	τ_0 (μs)[b]	τ_{air} (μs)[b]	F_T	Φ_Δ[c]
ChlE	10.2	110	0.25	>0.99	0.64
ChlE*[a]	19.9	141	0.35	>0.99	
Chl *a*	20.7	294	0.24	>0.99	0.66
Chl *b*	20.7	229	0.26	>0.99	

[a]ChlE irradiated with visible light from a 250 W Xe lamp (λ > 400 nm) for 60 min. [b]Estimated error less than 5%. [c]Estimated error less than 15%.

To remove the $O_2(^1\Delta_g)$ quenchers from the extract, purification by chromatographic methods was needed. Alternatively, we irradiated raw ChlE with visible light, under which the quenching effect of carotenoids was suppressed by their oxidation with $O_2(^1\Delta_g)$ to form photochemically inactive endoperoxides.[17] The value of τ_Δ also increased with increasing irradiation time up to a value of ~20.6 μs measured for the ZnPc standard, which corresponds with the literature data for THF (Figure 1B).[36] This effect corresponds with degradation of the quenchers through the reaction of $O_2(^1\Delta_g)$ with the double bonds of carotenoids. Note that carotenoids exhibit complex behaviors and can be degraded by other mechanisms, for example, by free radical reaction.[37,38] The changes in the absorbance of Q_y bands at 664 nm also indicate partial photodegradation of ChlE (proportional to changes in the absorbance of the Q_y band).

We also measured transient absorption spectra to evaluate the kinetics of the photosensitizer (predominantly Chl *a*) triplet states—a precursor of $O_2(^1\Delta_g)$ (Figure S5 in Supporting Information). The kinetics of the triplet states in THF show very efficient quenching of the triplets by dissolved oxygen (Table 2), leading to $O_2(^1\Delta_g)$ formation. We also found a lower lifetime of the photosensitizer triplet states for ChlE (167 μs) in argon-saturated THF in comparison with the Chl *a* standard (294 μs); however, more than 99% of triplets were quenched by oxygen in an air-saturated solution of ChlE, indicating that quenching by oxygen was dominant in comparison with quenching by carotenoids. Overall, the basic processes photosensitized by ChlE are summarized in Figure 2.

Photostability. A relatively photostable ChlE from the cyanobacterium *Spirulina maxima* was recently suggested for application in photodynamic therapy after purification.[39] We tested the photostability of our raw ChlE from spinach after irradiation with a 500 W Xe lamp with a long pass filter ($\lambda \geq$ 400 nm), and the kinetics of decomposition were followed at 664 and 459 nm (Figure 3). The first wavelength (664 nm) corresponds to the absorption bands of Chl, and the second wavelength (459 nm) corresponds to the absorption band of β-carotene. The photodegradation of β-carotene dominated, and the amount of β-carotene was negligible after 20 min of irradiation both in ChlE and in a two-component model, where standards of Chl *a* and β-carotene were mixed. The photodegradation of both Chl and β-carotene is a complex process, including oxidation by photogenerated $O_2(^1\Delta_g)$ and energy transfer from excited Chl *a* to β-carotene (Figure 2).[40]

A sample of ChlE after 50 min of irradiation was analyzed by HPLC. Chl *a* and Chl *b* were present in the sample, but no lutein or carotene was found (Figure S1, panel C in Supporting Information).

Sulfonated and Nonsulfonated Polystyrene Nanoparticles. *Preparation and Characterization.* Sulfonated and nonsulfonated polystyrene NPs were prepared by simple

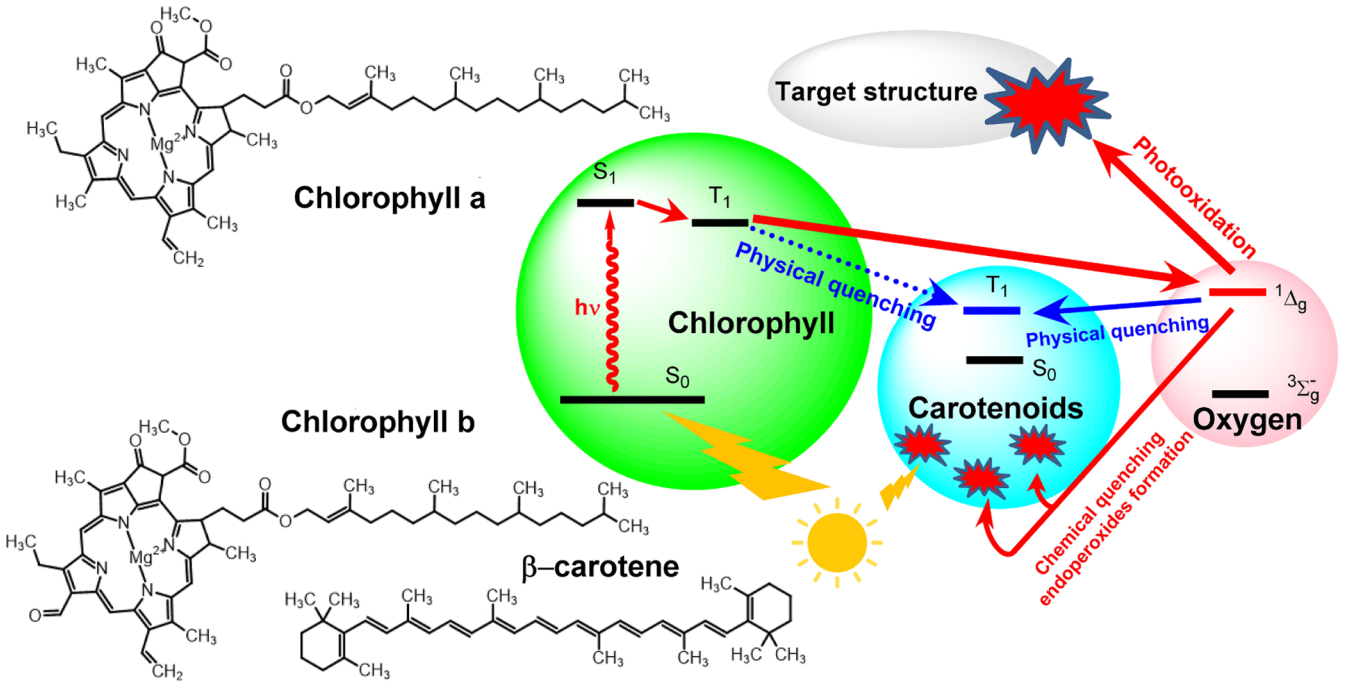

Figure 2. Simplified scheme of processes photosensitized by ChlE leading to photo-oxidation of target structures. Chl molecules were partially photodegraded during irradiation.

https://doi.org/10.1021/acsomega.1c06229
ACS Omega 2022, 7, 1505−1513

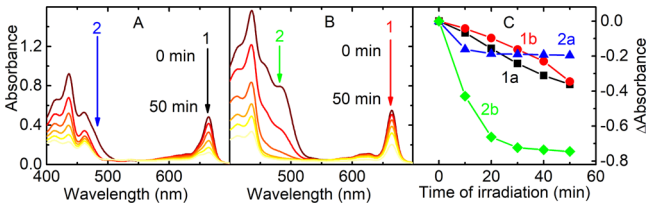

Figure 3. (A) Visible spectra of ChlE (corresponding to ~4.7 mg/L Chl *a*). (B) Visible spectra of a two-component model mixture of Chl *a* (5.3 mg/L) with *β*-carotene (51 mg/L) standards during irradiation. The absorption bands of chlorophyll *a* at 664 nm and carotene at 482 nm are assigned as (1) and (2), respectively. (C) Kinetics of photodegradation of Chl *a* in ChlE (1a) and in the model mixture with *β*-carotene (1b) and kinetics of photodegradation of *β*-carotene in ChlE (2a) and in the model mixture (2b). Irradiation was performed with a 500 W Xe lamp with a long pass filter ($\lambda \geq 400$ nm).

nanoprecipitation of THF solutions of sulfonated or nonsulfonated polystyrene enriched with THF spinach extract or standards/quenchers (see Experimental Section and Figure S6 in Supporting Information). Sulfonation of the polystyrene matrix increased NP stability, even in aqueous environments with high ionic strengths.[41]

The dispersions of sulfonated/nonsulfonated polystyrene NPs with spinach extract (ChlE@NPs) and NPs without and with the chlorophyll standard and carotene quencher were characterized by transmission electron microscopy (TEM) (Figure 4B,C), UV/vis absorption and fluorescence spectroscopy (Figure 4E), and dynamic light scattering (DLS) (Figure 4F).

The nanoprecipitation method led to mostly spherical NPs, as observed in the TEM images, where larger NPs were more visible in comparison to the bulk of small NPs revealed by DLS. The basic properties of the NPs are summarized in Table 3.

Dispersions of NPs prepared from nonsulfonated polystyrene nanofiber membranes displayed hydrodynamic diameters of approximately 230−280 nm. The sulfonated NPs had average hydrodynamic diameters of approximately 60−64 nm with a low polydispersity (PDI index of 0.2−0.3), in contrast to nonsulfonated NPs, where the freshly prepared nonsulfonated NPs were polydispersed with a tendency to precipitate. The size and zeta potential of NPs showed their high stability over time (Table S2 in Supporting Information).

According to HPLC analysis, the composition of encapsulated compounds in NPs corresponded to the composition of ChlE. Generally, chlorophylls are not stable in an acid environment and can undergo demetalation to the corresponding pheophytin but under our experimental conditions, no demetalation occurs (Figure S1, panel C in Supporting Information).

Also, no absorption or fluorescence of Chls was found in the filtrate (Figure S7 in Supporting Information), which indicates no leaching to aqueous media. The Soret absorption maximum of Chl *a* in the absorption spectrum of ChlE was shifted from 436 nm in THF solution to 415 nm in ChlE@NP dispersion.

Photophysical Properties. In contrast to a solution, individual components of ChlE (Chls and carotenoids) are fixed at specific places inside glassy ChlE@NPs, and only oxygen can diffuse through the polystyrene matrix[42] with a relatively high oxygen diffusion coefficient [$D(O_2) \sim 3\times10^7$ cm^{-1} s^{-1}].[43] The lifetime of singlet oxygen (τ_Δ) measured from weak NIR luminescence is controlled by the size of the NPs,[26] by different values of τ_Δ in the NP interior and outside in the aqueous environment, and by additional quenching by carotenoids (Figure 5a). Note that only $O_2(^1\Delta_g)$ that diffuses from the NP interior to the exterior environment can be used for photo-oxidation of chemical substrates and bacterial structures (see photo-oxidation tests and photodynamic inactivation of *Escherichia coli*). For this reason, polystyrene with a high oxygen diffusion coefficient was selected as the starting material for NP preparation.[43]

Prolongation of $O_2(^1\Delta_g)$ luminescence kinetics for sulfonated ChlE@NPs prepared from extract preirradiated with visible light from a Xe lamp, Figure 5c, τ_Δ = 13 μs) in

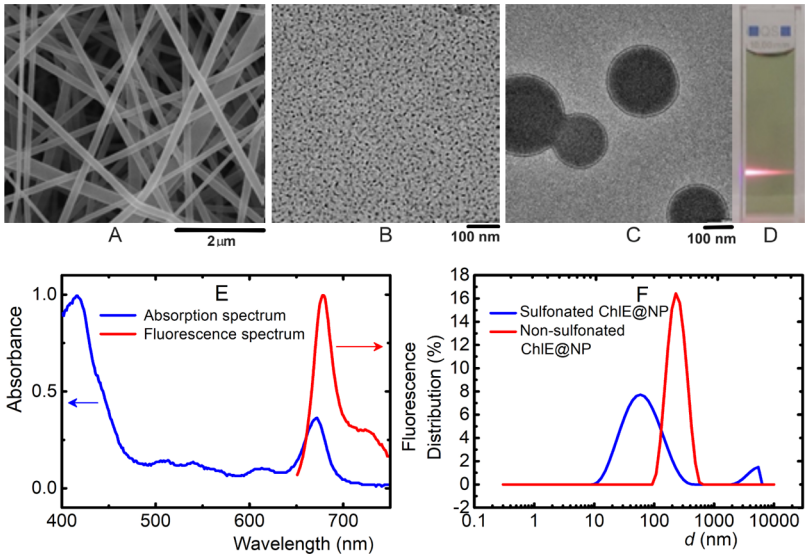

Figure 4. (A) SEM of pristine polystyrene nanofiber material for preparation of NPs, (B) TEM of sulfonated ChlE@NP dispersion, and (C) TEM of nonsulfonated ChlE@NP dispersion. (D) Photograph of a cell containing sulfonated ChE@NP dispersion with an impinging laser beam. (E) Absorption (a) and fluorescence (λ_{exc} = 417 nm) (b) spectra of sulfonated ChlE@NP dispersion. (F) DLS size distribution of sulfonated ChlE@NP and freshly prepared nonsulfonated ChlE@NP dispersion.

https://doi.org/10.1021/acsomega.1c06229
ACS Omega 2022, 7, 1505−1513

Table 3. Basic Properties of Sulfonated and Nonsulfonated NPs

	nonsulfonated NPs		sulfonated NPs			
properties	@NPs	ChlE@NPs	@NPs	ChlE@NPs	Chl*a*@NPs	Chl*a*Car@NPs
diameter (DLS) (nm)	278	227	64	61	60	60
zeta potential (mV)	−34	−31	−33	−26	−31	−34
number of NPs in 1 mL dispersion	2.60×10^{10}	4.48×10^{10}	1.41×10^{13}	2.02×10^{13}	1.98×10^{14}	
surface (nm^2)	243 000	162 000	13 000	12 000	11 000	11 000
surface/volume (nm^{-1})	0.02	0.03	0.09	0.10	0.10	0.10
appearance	milky	milky green	transparent	transparent green	transparent green	milky orange

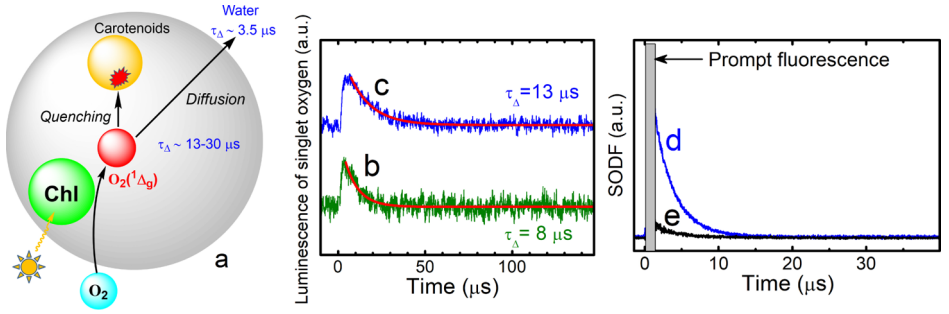

Figure 5. Simplified behavior of $O_2(^1\Delta_g)$ in the NP interior and outside NPs in an aqueous environment (a). Normalized singlet oxygen kinetics after excitation of ChlE in sulfonated ChlE@NPs (b) and preirradiated sulfonated ChlE@NPs (c). The SODF signal for preirradiated sulfonated (d) and nonsulfonated ChlE@NPs (e). Experiments were carried out in an oxygen-saturated water dispersion to increase the amount of $O_2(^1\Delta_g)$ generated by the photosensitization process. The red lines are single exponential fits to the experimental data. Note that the value of τ_Δ is influenced by slow decay kinetics of Chls triplets in nanoparticles (Figure S8 in Supporting Information).

comparison with NPs prepared from raw extract (Figure 5b, τ_Δ = 8 μs), indicated photodegradation of carotenoids and loss of both physical and chemical quenching properties.

Nonsulfonated ChlE@NPs did not provide any measurable $O_2(^1\Delta_g)$ luminescence signal. We used singlet oxygen-sensitized delayed fluorescence (SODF), a more sensitive method for detection of singlet oxygen inside NPs, that arises from the interaction of $O_2(^1\Delta_g)$ with the triplet states of photosensitizers.[44] The SODF signal at high excitation energy is a few orders of magnitude stronger than the weak luminescence of $O_2(^1\Delta_g)$ at 1270 nm and therefore can be used for detection of lower concentrations of $O_2(^1\Delta_g)$. Comparison of the SODF signals confirmed a dramatic decrease in the $O_2(^1\Delta_g)$ concentration for nonsulfonated ChlE@NPs (Figure 5e) compared with preirradiated sulfonated ChlE@NPs (Figure 5d). Even nonirradiated ChlE@NPs showed a much higher SODF signal (Figure S9 in Supporting Information). Recently, we found that the SODF signal increased with the average size of NPs loaded with a photosensitizer (porphyrin) as a consequence of an increased amount of communicating/interacting molecules of photosensitizers *via* photogenerated $O_2(^1\Delta_g)$.[41,44] In contrast to previous studies, the higher SODF signal for smaller sulfonated ChlE@NPs than for larger nonsulfonated ChlE@NPs is likely due to inhibition of SODF by carotenoid quenchers that reduce the concentration of $O_2(^1\Delta_g)$ inside ChlE@NPs.

Photostability. ChlE and both sulfonated and nonsulfonated ChlE@NPs in aqueous dispersion (6.9×10^{12} NPs/ml) were irradiated with visible light from a 500 W Xe lamp with a long pass filter ($\lambda \geq 400$ nm) to compare their photostability. The kinetics of Chl decomposition was followed at a wavelength of 664 nm, which corresponded to the absorption band of Chl *a*. The sulfonated ChlE@NPs exhibited similar photostability as ChlE itself that is in contrast to more stable nonsulfonated ChlE@NPs with smaller size and higher photo-oxidation efficiency (Figure S10, panel C in Supporting Information).

Photo-oxidation of Chemical Substrates. The dispersions of NPs were irradiated with a 36 W red light-emitting diode (LED) grow light bulb (λ = 662 nm) in iodide detection solution to observe $O_2(^1\Delta_g)$ photogeneration (see Experimental Section). A linear increase in the I_3^- concentration (following the UV/vis absorbance change at 287 or 351 nm) proportional to the generation of $O_2(^1\Delta_g)$[45] was found (Figure S11 in Supporting Information). Alternatively, $O_2(^1\Delta_g)$ photogeneration was confirmed by photodegradation of uric acid at 293 nm[46] (Figure S12 in Supporting Information). The experimental data indicate that oxidation of both I^- and uric acid substrates is due to oxidation by $O_2(^1\Delta_g)$ for several reasons: a) formation of $O_2(^1\Delta_g)$ was confirmed from luminescence measurement (see photophysical measurements above), (b) the oxidation did not take place in inert gas-saturated samples and/or in aerated samples in the dark, and (c) a strong physical quencher of singlet oxygen (sodium azide)[47] inhibited oxidation of both substrates.

A fluorescence assay using terephthalic acid[48] did not reveal the generation of any other ROS (H_2O_2, O_2^-, and $OH^\cdot$). Also, no post-irradiation effect, for example, dark oxidation of iodide (in iodide test), typical for accumulation of H_2O_2 due to presence of OH and O_2^- was found. However, we cannot exclude the minor formation of these species; the quantitative evaluation of data for such complex systems may be limited.[49]

To estimate the relative efficiency of I^- photo-oxidation to I_3^- by $O_2(^1\Delta_g)$, absorbance-matched dispersions of different NPs were irradiated with a red LED bulb (λ = 662 nm). Figure 6 shows that smaller sulfonated ChlE@NPs were much more effective producers of $O_2(^1\Delta_g)$ than larger, nonsulfonated ChlE@NPs and exhibited approximately the same photo-oxidation efficiency as Chl*a*@NPs (using a Chl *a* analytical standard) of a similar size.

https://doi.org/10.1021/acsomega.1c06229
ACS Omega 2022, 7, 1505−1513

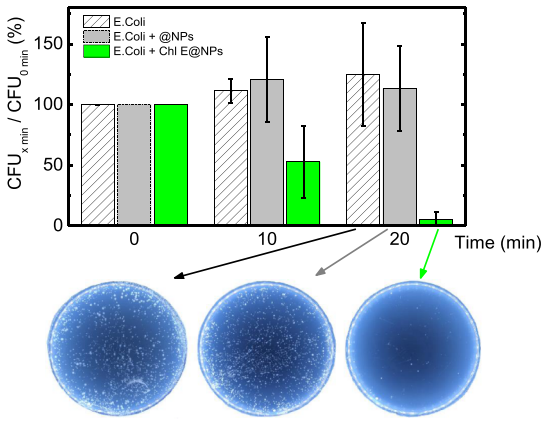

Figure 6. Absorption spectra of Chl*a*@NPs (a), sulfonated ChlE@NPs (b), Chl*a*Car@NPs (c), and nonsulfonated ChlE@NPs (d). Relative photo-oxidation efficiency estimated as absorbance changes at 351 nm that corresponds to the I_3^- absorption band in the photo-oxidation of I^- by $O_2(^1\Delta_g)$ using sulfonated Chl*a*@NPs (e), ChlE@NPs (f), Chl*a*Car@NPs (g), and nonsulfonated ChlE@NPs (h). The measurements were carried out with absorbance-matched samples at an excitation wavelength of 662 nm; samples were irradiated with a red LED bulb (λ = 662 nm).

The presence of β-carotene reduces the photo-oxidation response. Surprisingly, we found that sulfonated Chl*a*Car@NPs (originating from 4 mg of β-carotene) have the same photo-oxidation kinetics as a sample with a half concentration of β-carotene (2 mg, not shown). This observation may correspond with the small size of NPs: $O_2(^1\Delta_g)$ photogenerated near the surface of NPs is directly released into aqueous media and does not meet any β-carotene (carotenoid) quencher located inside the NPs. In contrast, $O_2(^1\Delta_g)$ photogenerated inside larger nonsulfonated NPs can be quenched even by a low concentration of β-carotene. This efficient quenching reduces the number of $O_2(^1\Delta_g)$ molecules that diffuse into the environment of the NPs toward target structures and inhibits total photo-oxidation (Figure 6).

To evaluate the preirradiation effect on the relative efficiency of photo-oxidation of chemical/biological targets by $O_2(^1\Delta_g)$, aqueous dispersions of sulfonated ChlE@NPs and nonsulfonated ChlE@NPs were irradiated with a 36 W red LED bulb before addition of iodide detection solution and photo-oxidation tests. Preirradiation of sulfonated ChlE@NPs led only to a decrease in photo-oxidation efficiency, attributed to the common photodegradation of Chl photosensitizers (Figure S13 in Supporting Information). The large nonsulfonated ChlE@NPs exhibited a more complex profile with limited reproducibility.

In our previous study,[41] we found that polystyrene NPs can be easily removed by filtration through a 0.03 mm thin hydrophilic electrospun polyurethane (Tecophilic) nanofiber membrane. The removal of sulfonated ChlE@NPs was followed by decreased red fluorescence in the supernatant (Figure S7 in Supporting Information). After one filtration, approximately 90% of fluorescent ChlE@NPs were removed. Repeated filtration yielded complete removal of all NPs. No fluorescence or absorption was observed, and only a background DLS signal was observed. This test also verified that the hydrophobic compounds in ChlE are fixed in the glassy polystyrene matrix, which efficiently prevents release of the encapsulated compounds into the aqueous medium. In short, only components of ChlE encapsulated in ChlE@NPs exhibited an efficient photoantibacterial effect due to the formation of cytotoxic $O_2(^1\Delta_g)$.

Photodynamic Inactivation of E. coli. Previous photo-oxidation experiments revealed that $O_2(^1\Delta_g)$-generating NPs can easily oxidize external substrates in aqueous media. To test photodynamic inactivation (PDI), a suspension of Gram-negative *E. coli* was mixed with a dispersion of @NPs or sulfonated ChlE@NPs and irradiated with a 36 W red LED bulb (λ = 662 nm) for 0, 10, and 20 min. No significant photodegradation of Chls during irradiation (monitored by changes in the absorbance at 664 nm) was observed (Figure S10 in Supporting Information). In contrast to controls (suspension of *E. coli* alone or with sulfonated @NPs), a substantial decrease in the colony forming unit (CFU) ratio was observed when sulfonated ChlE@NPs were used (Figure 7). ChlE@NPs kept in the dark also exhibited no antibacterial

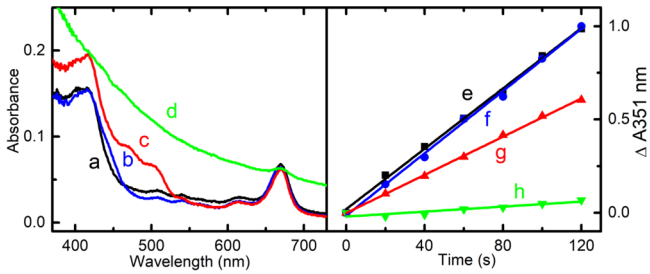

Figure 7. (Photo)antibacterial activity estimated as the average number of CFUs of *E. coli* observed on agar plates after irradiation with visible light. The average number of CFUs corresponding to treatment of *E. coli* alone (dashed), *E. coli* with @NPs (gray), and *E. coli* with sulfonated ChlE@NPs (green) after 0, 10, and 20 min of irradiation versus samples stored in the dark based on three independent tests, and photographs of agar plates. Irradiation source: 36 W red LED bulb (λ = 662 nm).

effect (Table S3 in Supporting Information). In contrast to the frequently observed antibacterial effect of visible light itself (especially in the blue region), we found a slight increase in the CFU ratio. This stimulation effect can be attributed to the temperature increase in the cuvette chamber (0.5−1.0 °C) during irradiation.

CONCLUSIONS

Polystyrene nanoparticles with Chl photosensitizers from green plants prepared by simple nanoprecipitation methods can be inexpensive and green alternatives to photoactive antimicrobial NPs with many applications, for example, for cleaning contaminated water or for antibacterial treatment of biofilms. The high quantum yield of singlet oxygen generation for ChlE (close to that of pure Chl *a*) allows direct application in photodynamic treatment without a complicated purification process to prepare individual photosensitizers. The quenching effect of carotenoids in ChlE can be suppressed by preirradiation with visible light, under which carotenoids decompose more efficiently than Chl photosensitizers and lose their quenching ability due to the reaction of $O_2(^1\Delta_g)$ with the conjugated double bonds of carotenoids. Encapsulation of Chl photosensitizers from ChlE in polystyrene NPs led to higher photostability. NPs prepared from sulfonated polystyrene with small sizes (diameter of ∼60 nm) exhibited more efficient photo-oxidation and antibacterial properties than those prepared from nonsulfonated polystyrene. Moreover, efficient

https://doi.org/10.1021/acsomega.1c06229
ACS Omega 2022, 7, 1505−1513

removal of the NPs together with the inactivated bacteria after their use by simple filtration through an electrospun membrane (a precursor of NPs) is also an important benefit.

EXPERIMENTAL SECTION

Materials. Chl (Chl *a* and Chl *b*), lutein, and *β*-carotene standards; uric acid sodium salt; tetraethylammonium bromide (TEAB); hydrogen peroxide; ampicillin; potassium iodide and other inorganic salts (all Sigma-Aldrich); phosphate-buffered saline (PBS); agar and LB medium (Lennox) (all Carl Roth GmbH); cyclohexanone; and sulfuric acid (both Lach-Ner, Czech Republic) were used as delivered. THF (Sigma-Aldrich) was dried with a PureSolv MD5 solvent purification system (Innovative Technology). PS GP 137 polystyrene was purchased from Synthos Kralupy (Czech Republic). ChlE was prepared from spinach. Spinach leaves [100 g, Italy: grown in a greenhouse, baby spinach (Spinacia), summer] were dried at room temperature between filter papers in the dark for 2 weeks. ChlE was prepared from 17.5 g of dried leaves extracted with 200 mL THF, filtered and used for experiments without any other purification.

Preparation of Nanofiber Material and NPs. A mixture of 0.07 wt % TEAB and 99.93 wt % polystyrene was dissolved in cyclohexanone to prepare a 17% solution for fabrication of electrospun polystyrene nanofiber material. The conductivity of the solution was enhanced by TEAB (0.12 g/kg). The electrospinning process was described in detail in our previous papers.[25,43,50]

Sulfonated NPs were prepared from electrospun polystyrene nanofiber material fixed on quartz substrates treated with immersion in 96% sulfuric acid[41] at room temperature for 48 h. The materials were washed with distilled water until a neutral pH was reached and were then stored between two pieces of polypropylene fabric cover. Typically, a gently wet, sulfonated nanofiber membrane (16 mg) was immersed in 4 mL of dry THF with ChlE (ca 0.2 mg) or Chl *a* standard (0.2 mg) or *β*-carotene standards (2.0 mg) for 60 s with stirring; then, distilled water (20 mL) was added. The concentration of standards was checked using extinction coefficients (Table S1 in Supporting Information). THF was removed by evaporation under a slight vacuum (60 °C, to a final volume of approximately 15 mL). The resulting dispersion of NPs in water was centrifuged for 10 min at 3070 g to remove microparticles and was dialyzed using Float-A-Lyzer G2 with a molecular weight cutoff of 50 kDa for 15 h in distilled water at room temperature to remove traces of sulfuric acid and THF. Nonsulfonated NPs were prepared under the same protocol (see above) without sulfonation.

HPLC Analysis. HPLC analyses were performed on an Agilent Infinity 1290 liquid chromatographic system coupled with a Triple Quad 6460 tandem mass spectrometric detection system (Agilent Technologies, Germany). A SunFire C18 column (150 mm × 4.6 mm, 5 μm particle size), (Waters, Ireland), thermostatted at 20 °C, was used for separation. The mobile phase consisted of methanol (MeOH) with 0.5% formic acid at a flow rate of 0.8 mL/min. The injection volume was 20 μL, and samples were kept at 20 °C. The MS/MS measurements were performed in the multiple reaction-monitoring (MRM) mode using positive electrospray ionization (ESI). The gas flow was 10 L/min, gas temperature was 350 °C, nebulizer pressure was 55 psi, and capillary voltage was 5500 V. The optimized MS/MS conditions are shown in Table S4 in the Supporting Information. Total-ion current (TIC) chromatograms with MRM chromatograms of the individual analytes obtained for a mixture of standards are shown in Figure S1, panel A (Supporting Information), and the same TIC chromatograms recorded for ChlE are shown in Figure S1, panel B (Supporting Information).

Characterization of NPs and Electrospun Polymeric Membranes. Nanofiber and NP morphology was studied with a scanning electron Quanta 200 FEG microscope (FEI, Czech Republic). The nanofiber diameters were measured using NIS Elements 4.0 image analysis software (Laboratory Imaging, Czech Republic). The NP size and size distributions in water were determined by dynamic light scattering on a Zetasizer Nano ZS particle size analyzer from Malvern (United Kingdom).

Photophysical Properties. UV/vis absorption spectra were recorded using Unicam 340 and Varian 4000 spectrometers. The steady-state fluorescence spectra were monitored using an FLS 980 (Edinburgh Instruments, UK) spectrofluorimeter. For time-resolved measurements, the samples were excited with a Lambda Physik FL3002 laser (λ_{exc} = 664 nm and pulse length ∼28 ns) that matched the Q_y band of Chls[51] in the extract and both Chl *a* and zinc phthalocyanine (ZnPc) standards. Time-resolved near-infrared luminescence of $O_2(^1\Delta_g)$ at 1270 nm was observed using a homemade detector unit (interference filters, Ge diode). Temporal profiles of $O_2(^1\Delta_g)$ luminescence were averaged and calculated as the difference between signals in oxygen- and argon-saturated H_2O. They were fitted to a single exponential function: $I = I_0 \exp(-t/\tau_\Delta)$, in which τ_Δ is the lifetime of singlet oxygen. The fitting procedure excluded the initial part of the plot influenced by light scattering and fluorescence (usually 1−2 μs after excitation). The details can be found in our previous paper.[26] Transient absorption spectra of photosensitizers (corresponding to triplet−triplet transitions) and decay kinetics of the photosensitizer triplet states were measured on an LKS 20 laser kinetic spectrometer (Applied Photophysics, United Kingdom) in oxygen-, air-, and argon-saturated solvents/dispersions.

Photo-oxidation Properties. A dispersion of NPs with or without encapsulated ChlE, Chl *a*, or *β*-carotene (∼1.3×10^{12} NPs/mL for sulfonated NPs and ∼1.5×10^{9} NPs/mL for nonsulfonated NPs) was placed in a thermostatted 10 mm quartz cell (22 °C) that contained 0.1 M iodide detection solution or 2×10^{-4} M uric acid in 0.02 M phosphate buffer (pH = 7.0). The cell was irradiated with visible light using a stabilized xenon lamp (500 W, Newport) with a long pass filter ($\lambda \geq 400$ nm, Newport) or using a 36 W LED bulb with an emission at 662 nm (for spectral irradiance see Figure S14 in Supporting Information). The UV/vis absorbance changes at 287 or 351 nm (attributed to the formation of I_3^- in the iodide test)[45] or 291 nm (attributed to photodegradation of uric acid)[52,53] were recorded at regular intervals and compared to a blank solution of the same composition that was stored in the dark. Spectral and total irradiance of the used light sources was evaluated with an ILT960 spectroradiometer SpectriLight (International Light Technologies, USA).

Antibacterial Assays. A culture of *E. coli* DH5α (Invitrogen, CA, USA) with the plasmid pGEM11Z (Promega, WI, USA) was incubated at 37 °C while stirring in LB medium after addition of ampicillin. Incubation was terminated when the absorbance at 560 nm reached approximately 1.2. The prepared culture was diluted 5000× to the desired concentration in PBS. NPs from stock suspensions of sulfonated NPs

https://doi.org/10.1021/acsomega.1c06229
ACS Omega 2022, 7, 1505−1513

(~2.0 × 10^{13} NPs/mL) with or without encapsulated ChlE were mixed with diluted bacterial culture at a ratio of 1:1. Two milliliters of this suspension was placed in a thermostatted 10 mm quartz cell (25 °C). While stirring, the cell was irradiated with red light produced by a stabilized deep red LED grow light bulb (36 W and 662 nm). At regular time intervals, 150 μL of the irradiated suspension was placed on an agar plate. The plates were incubated for 20 h in darkness at 37 °C to allow the individual bacteria to grow and form colonies.[41]

■ ASSOCIATED CONTENT

Supporting Information

The Supporting Information is available free of charge at https://pubs.acs.org/doi/10.1021/acsomega.1c06229.

HPLC analysis, absorption and fluorescence spectra, time-resolved luminescence of $O_2(^1\Delta_g)$, transient absorption data, delayed fluorescence of ChlE from spinach, and nanoparticles prepared from ChlE from spinach (PDF)

■ AUTHOR INFORMATION

Corresponding Authors

Pavel Kubát − *J. Heyrovský Institute of Physical Chemistry of the Czech Academy of Sciences, 182 23 Prague 8, Czech Republic*; orcid.org/0000-0002-7861-9212; Email: pavel.kubat@jh-inst.cas.cz

Jiří Mosinger − *Faculty of Science, Charles University, 128 43 Prague 2, Czech Republic*; orcid.org/0000-0001-5173-2744; Email: mosinger@natur.cuni.cz

Authors

Pavel Ludačka − *Faculty of Science, Charles University, 128 43 Prague 2, Czech Republic*

Zuzana Bosáková − *Faculty of Science, Charles University, 128 43 Prague 2, Czech Republic*

Complete contact information is available at: https://pubs.acs.org/10.1021/acsomega.1c06229

Notes

The authors declare no competing financial interest.

■ ACKNOWLEDGMENTS

This work was supported by the Czech Science Foundation (19−09721S) and by the OP VVV "Excellent Research Teams", project no. CZ.02.1.01/0.0/0.0/15_003/0000417−CUCAM. The authors thank Dr. Miroslav Štěpánek for TEM evaluation of NPs and Dr. Pavel Engst for help with the photophysical measurements.

■ ABBREVIATIONS

Chl *a*	chlorophyll *a*
Chl *b*	chlorophyll *b*
ChlE	chlorophyll extract from spinach in THF
ChlE*	designates ChlE preirradiated with a Xe lamp with a long pass filter (λ > 400 nm)
NPs	nanoparticles
@NPs	nanoparticles without a phototosensitizer
Chlx@NPs	polystyrene nanoparticles with chlorophyll *a* or chlorophyll extract (x = *a*, E)
Chl*a*Car@NPs	polystyrene nanoparticles with both chlorophyll *a* and β-carotene

■ REFERENCES

(1) Kotkowiak, M.; Dudkowiak, A.; Fiedor, L. Intrinsic Photoprotective Mechanisms in Chlorophylls. *Angew. Chem., Int. Ed.* **2017**, *56*, 10457−10461.

(2) Vinklárek, I. S.; Bornemann, T. L. V.; Lokstein, H.; Hofmann, E.; Alster, J.; Pšenčík, J. Temperature Dependence of Chlorophyll Triplet Quenching in Two Photosynthetic Light-Harvesting Complexes from Higher Plants and Dinoflagellates. *J. Phys. Chem. B* **2018**, *122*, 8834−8845.

(3) Schilling, W.; Zhang, Y.; Sahoo, P. K.; Sarkar, S. K.; Gandhi, S.; Roesky, H. W.; Das, S. Nature inspired singlet oxygen generation to access α-amino carbonyl compounds via 1,2-acyl migration. *Green Chem.* **2021**, *23*, 379−387.

(4) Krieger-Liszkay, A. Singlet oxygen production in photosynthesis. *J. Exp. Bot.* **2004**, *56*, 337−346.

(5) Dogra, V.; Kim, C. Singlet Oxygen Metabolism: From Genesis to Signaling. *Front. Plant Sci.* **2019**, *10*, 1640.

(6) Hamblin, M. R.; Hasan, T. Photodynamic therapy: a new antimicrobial approach to infectious disease? *Photochem. Photobiol. Sci.* **2004**, *3*, 436−450.

(7) Maisch, T.; Baier, J.; Franz, B.; Maier, M.; Landthaler, M.; Szeimies, R.-M.; Bäumler, W. The role of singlet oxygen and oxygen concentration in photodynamic inactivation of bacteria. *Proc. Natl. Acad. Sci. U.S.A* **2007**, *104*, 7223−7228.

(8) Agostinis, P.; Berg, K.; Cengel, K. A.; Foster, T. H.; Girotti, A. W.; Gollnick, S. O.; Hahn, S. M.; Hamblin, M. R.; Juzeniene, A.; Kessel, D.; Korbelik, M.; Moan, J.; Mroz, P.; Nowis, D.; Piette, J.; Wilson, B. C.; Golab, J. Photodynamic therapy of cancer: an update. *Ca-Cancer J. Clin.* **2011**, *61*, 250−281.

(9) Lo, P.-C.; Rodríguez-Morgade, M. S.; Pandey, R. K.; Ng, D. K. P.; Torres, T.; Dumoulin, F. The unique features and promises of phthalocyanines as advanced photosensitisers for photodynamic therapy of cancer. *Chem. Soc. Rev.* **2020**, *49*, 1041−1056.

(10) Campanholi, K. d. S. S.; Braga, G.; da Silva, J. B.; da Rocha, N. L.; de Francisco, L. M. B.; de Oliveira, É. L.; Bruschi, M. L.; de Castro-Hoshino, L. V.; Sato, F.; Hioka, N.; Caetano, W. Biomedical Platform Development of a Chlorophyll-Based Extract for Topic Photodynamic Therapy: Mechanical and Spectroscopic Properties. *Langmuir* **2018**, *34*, 8230−8244.

(11) Wilkinson, F.; Helman, W. P.; Ross, A. B. Quantum Yields for the Photosensitized Formation of the Lowest Electronically Excited Singlet State of Molecular Oxygen in Solution. *J. Phys. Chem. Ref. Data* **1993**, *22*, 113−262.

(12) Redmond, R. W.; Gamlin, J. N. A Compilation of Singlet Oxygen Yields from Biologically Relevant Molecules. *Photochem. Photobiol.* **1999**, *70*, 391−475.

(13) Tamura, H.; Ishikita, H. Quenching of Singlet Oxygen by Carotenoids via Ultrafast Superexchange Dynamics. *J. Phys. Chem. A* **2020**, *124*, 5081−5088.

(14) Demmig-Adams, B.; Gilmore, A. M.; Adams, W. W., III In vivo functions of carotenoids in higher plants. *FASEB J.* **1996**, *10*, 403−412.

(15) Croce, R.; Van Amerongen, H. Natural strategies for photosynthetic light harvesting. *Nat. Chem. Biol.* **2014**, *10*, 492−501.

(16) Demmig-Adams, B. Carotenoids and photoprotection in plants: A role for the xanthophyll zeaxanthin. *Biochim. Biophys. Acta Bioenerg.* **1990**, *1020*, 1−24.

(17) Ramel, F.; Birtic, S.; Cuiné, S.; Triantaphylidès, C.; Ravanat, J.-L.; Havaux, M. Chemical Quenching of Singlet Oxygen by Carotenoids in Plants. *Plant Physiol.* **2012**, *158*, 1267−1278.

(18) Peterman, E.; Monshouwer, R.; van Stokkum, I. H. M.; van Grondelle, R.; van Amerongen, H. Ultrafast singlet excitation transfer from carotenoids to chlorophylls via different pathways in light-harvesting complex II of higher plants. *Chem. Phys. Lett.* **1997**, *264*, 279−284.

(19) Barazzouk, S.; Bekalé, L.; Hotchandani, S. Enhanced photostability of chlorophyll-a using gold nanoparticles as an efficient photoprotector. *J. Mater. Chem.* **2012**, *22*, 25316−25324.

(20) Bobbio, P. A.; Guedes, M. C. Stability of copper and magnesium chlorophylls. *Food Chem.* **1990**, *36*, 165−168.
(21) Küpper, H.; Dědic, R.; Svoboda, A.; Hála, J.; Kroneck, P. M. H. Kinetics and efficiency of excitation energy transfer from chlorophylls, their heavy metal-substituted derivatives, and pheophytins to singlet oxygen. *Biochim. Biophys. Acta, Gen. Subj.* **2002**, *1572*, 107−113.
(22) Uliana, M. P.; Pires, L.; Pratavieira, S.; Brocksom, T. J.; de Oliveira, K. T.; Bagnato, V. S.; Kurachi, C. Photobiological characteristics of chlorophyll a derivatives as microbial PDT agents. *Photochem. Photobiol. Sci.* **2014**, *13*, 1137−1145.
(23) Ryberg, E. C.; Knight, J.; Kim, J.-H. Farm-to-Tap Water Treatment: Naturally-Sourced Photosensitizers for Enhanced Solar Disinfection of Drinking Water. *ACS ES&T Eng.* **2021**, *1*, 86−99.
(24) Lim, E.-K.; Kim, T.; Paik, S.; Haam, S.; Huh, Y.-M.; Lee, K. Nanomaterials for Theranostics: Recent Advances and Future Challenges. *Chem. Rev.* **2015**, *115*, 327−394.
(25) Henke, P.; Dolanský, J.; Kubát, P.; Mosinger, J. Multifunctional Photosensitizing and Biotinylated Polystyrene Nanofiber Membranes/Composites for Binding of Biologically Active Compounds. *ACS Appl. Mater. Interfaces* **2020**, *12*, 18792−18802.
(26) Kubát, P.; Henke, P.; Raya, R. K.; Štěpánek, M.; Mosinger, J. Polystyrene and Poly(ethylene glycol)-b-Poly(ε-caprolactone) Nanoparticles with Porphyrins: Structure, Size, and Photooxidation Properties. *Langmuir* **2020**, *36*, 302−310.
(27) Laxminarayan, R.; Duse, A.; Wattal, C.; Zaidi, A. K. M.; Wertheim, H. F. L.; Sumpradit, N.; Vlieghe, E.; Hara, G. L.; Gould, I. M.; Goossens, H.; Greko, C.; So, A. D.; Bigdeli, M.; Tomson, G.; Woodhouse, W.; Ombaka, E.; Peralta, A. Q.; Qamar, F. N.; Mir, F.; Kariuki, S.; Bhutta, Z. A.; Coates, A.; Bergstrom, R.; Wright, G. D.; Brown, E. D.; Cars, O. Antibiotic resistance-the need for global solutions. *Lancet Infect. Dis.* **2013**, *13*, 1057−1098.
(28) Wolfbeis, O. S. An overview of nanoparticles commonly used in fluorescent bioimaging. *Chem. Soc. Rev.* **2015**, *44*, 4743−4768.
(29) Gerola, A. P.; Costa, P. F. A.; de Morais, F. A. P.; Tsubone, T. M.; Caleare, A. O.; Nakamura, C. V.; Brunaldi, K.; Caetano, W.; Kimura, E.; Hioka, N. Liposome and polymeric micelle-based delivery systems for chlorophylls: Photodamage effects on Staphylococcus aureus. *Colloids Surf., B* **2019**, *177*, 487−495.
(30) Costa, P. F. A.; Gerola, A. P.; Pereira, P. C. S.; Souza, B. S.; Caetano, W.; Fiedler, H. D.; Nome, F.; Hioka, N. Chlorophylls B formulated in nanostructured colloidal solutions: Interaction, spectroscopic, and photophysical studies. *J. Mol. Liq.* **2019**, *274*, 393−401.
(31) Falco, W. F.; Botero, E. R.; Falcão, E. A.; Santiago, E. F.; Bagnato, V. S.; Caires, A. R. L. In vivo observation of chlorophyll fluorescence quenching induced by gold nanoparticles. *J. Photochem. Photobiol., A* **2011**, *225*, 65−71.
(32) Falco, W. F.; Queiroz, A. M.; Fernandes, J.; Botero, E. R.; Falcão, E. A.; Guimarães, F. E. G.; M'Peko, J.-C.; Oliveira, S. L.; Colbeck, I.; Caires, A. R. L. Interaction between chlorophyll and silver nanoparticles: A close analysis of chlorophyll fluorescence quenching. *J. Photochem. Photobiol., A* **2015**, *299*, 203−209.
(33) Cogdell, R. J.; Osmond, C. B.; Foyer, C. H.; Bock, G.; Howard, T. D.; Bittl, R.; Schlodder, E.; Geisenheimer, I.; Lubitz, W. How carotenoids protect bacterial photosynthesis. *Philos. Trans. R. Soc., B* **2000**, *355*, 1345−1349.
(34) Zielewicz, W.; Wróbel, B.; Niedbała, G. Quantification of Chlorophyll and Carotene Pigments Content in Mountain Melick (Melica nutans L.) in Relation to Edaphic Variables. *Forests* **2020**, *11*, 1197.
(35) Kaestner, L.; Cesson, M.; Kassab, K.; Christensen, T.; Edminson, P. D.; Cook, M. J.; Chambrier, I.; Jori, G. Zinc octa-n-alkyl phthalocyanines in photodynamic therapy: Photophysical properties, accumulation and apoptosis in cell cultures, studies in erythrocytes and topical application to Balb/c mice skin. *Photochem. Photobiol. Sci.* **2003**, *2*, 660−667.
(36) Sagadevan, A.; Hwang, K. C.; Su, M.-D. Singlet oxygen-mediated selective C-H bond hydroperoxidation of ethereal hydrocarbons. *Nat. Commun.* **2017**, *8*, 1812.
(37) Mordi, R. C.; Ademosun, O. T.; Ajanaku, C. O.; Olanrewaju, I. O.; Walton, J. C. Free Radical Mediated Oxidative Degradation of Carotenes and Xanthophylls. *Molecules* **2020**, *25*, 1038.
(38) Edge, R.; Truscott, T. Singlet Oxygen and Free Radical Reactions of Retinoids and Carotenoids-A Review. *Antioxidants* **2018**, *7*, 5.
(39) Martins, M.; Albuquerque, C. M.; Pereira, C. F.; Coutinho, J. A. P.; Neves, M. G. P. M. S.; G. A. Pinto, D. C.; Faustino, M. A. F.; Ventura, S. P. M.; Ventura, S. P. M. Recovery of Chlorophyll a Derivative from Spirulina maxima: Its Purification and Photosensitizing Potential. *ACS Sustain. Chem. Eng.* **2021**, *9*, 1772−1780.
(40) Hartzler, D. A.; Niedzwiedzki, D. M.; Bryant, D. A.; Blankenship, R. E.; Pushkar, Y.; Savikhin, S. Triplet Excited State Energies and Phosphorescence Spectra of (Bacterio)Chlorophylls. *J. Phys. Chem. B* **2014**, *118*, 7221−7232.
(41) Henke, P.; Kirakci, K.; Kubát, P.; Fraiberk, M.; Forstová, J.; Mosinger, J. Antibacterial, Antiviral, and Oxygen-Sensing Nanoparticles Prepared from Electrospun Materials. *ACS Appl. Mater. Interfaces* **2016**, *8*, 25127−25136.
(42) Poulsen, L.; Ogilby, P. R. Oxygen Diffusion in Glassy Polymer Films:Effects of Other Gases and Changes in Pressure. *J. Phys .Chem .A* **2000**, *104*, 2573−2580.
(43) Jesenská, S.; Plíštil, L.; Kubát, P.; Lang, K.; Brožová, L.; Popelka, Š.; Szatmáry, L.; Mosinger, J. Antibacterial nanofiber materials activated by light. *J. Biomed. Mater. Res., Part A* **2011**, *99*, 676−683.
(44) Kubát, P.; Henke, P.; Berzediová, V.; Štěpánek, M.; Lang, K.; Mosinger, J. Nanoparticles with Embedded Porphyrin Photosensitizers for Photooxidation Reactions and Continuous Oxygen Sensing. *ACS Appl. Mater. Interfaces* **2017**, *9*, 36229−36238.
(45) Mosinger, J.; Mosinger, B. Photodynamic sensitizers assay: rapid and sensitive iodometric measurement. *Experientia* **1995**, *51*, 106−109.
(46) Bregnhøj, M.; Dichmann, L.; McLoughlin, C. K.; Westberg, M.; Ogilby, P. R. Uric Acid: A Less-than-Perfect Probe for Singlet Oxygen. *Photochem. Photobiol.* **2019**, *95*, 202−210.
(47) Li, M. Y.; Cline, C. S.; Koker, E. B.; Carmichael, H. H.; Chignell, C. F.; Bilski, P. Quenching of Singlet Molecular Oxygen (1O2) by Azide Anion in Solvent Mixtures¶. *Photochem. Photobiol.* **2001**, *74*, 760−764.
(48) Leichnitz, S.; Heinrich, J.; Kulak, N. A fluorescence assay for the detection of hydrogen peroxide and hydroxyl radicals generated by metallonucleases. *Chem. Commun.* **2018**, *54*, 13411−13414.
(49) Lemp, E.; Zanocco, A. L.. *Singlet Oxygen: Applications in Biosciences and Nanosciences*; The Royal Society of Chemistry, 2016; Vol. *Volume 2Vol. 2*, pp 83−101.Chapter 29. Singlet Oxygen Chemical Acceptors DOI: 10.1039/9781782626992-00083
(50) Henke, P.; Lang, K.; Kubát, P.; Sýkora, J.; Šlouf, M.; Mosinger, J. Polystyrene Nanofiber Materials Modified with an Externally Bound Porphyrin Photosensitizer. *ACS Appl. Mater. Interfaces* **2013**, *5*, 3776−3783.
(51) Reimers, J. R.; Cai, Z.-L.; Kobayashi, R.; Rätsep, M.; Freiberg, A.; Krausz, E. Assignment of the Q-Bands of the Chlorophylls: Coherence Loss via Qx − Qy Mixing. *Sci. Rep.* **2013**, *3*, 2761.
(52) Iida, S.; Ohkubo, Y.; Yamamoto, Y.; Fujisawa, A. Parabanic acid is the singlet oxygen specific oxidation product of uric acid. *J. Clin. Biochem. Nutr.* **2017**, *61*, 169−175.
(53) Fischer, F.; Graschew, G.; Sinn, H.-J.; Maier-Borst, W.; Lorenz, W. J.; Schlag, P. M. A chemical dosimeter for the determination of the photodynamic activity of photosensitizers. *Clin. Chim. Acta* **1998**, *274*, 89−104.

https://doi.org/10.1021/acsomega.1c06229
ACS Omega 2022, 7, 1505−1513